Digital Signal Processing 60 (2017) 140–151

Contents lists available at ScienceDirect

Digital Signal Processing

www.elsevier.com/locate/dsp

Improvement of the visibility of concealed features in artwork NIR reflectograms by information separation

Jan Blažek [a,*], Jana Striová [b], Raffaella Fontana [b], Barbara Zitová [a]

[a] Institute of Information Theory and Automation of the CAS, Pod Vodárenskou věží 4, 182 08, Prague, Czech Republic
[b] National Institute of Optics, National Research Council, Largo Fermi 6, 50125, Florence, Italy

ARTICLE INFO

Article history:
Available online 21 September 2016

Keywords:
Signal separation
Painted layer enhancement
Separability limitations
Artwork analysis
Infrared reflectography

ABSTRACT

Near Infrared (NIR) reflectography, coupled to visible (VIS) one, is a spectrophotometric imaging technique employed to probe both the inner and the outer layers of artworks. NIR reflectograms may partially contain information pertinent to the visible spectrum (due to the poor pigment transparency in NIR) and this decreases their comprehensibility. This work presents an innovative digital processing methodology for accentuating information contained in the infrared reflectograms. The proposed method consists of inducing minor changes in pixel intensity by suppressing VIS information content from NIR information content. The method creates such enhanced NIR reflectogram by extrapolating VIS reflectogram to a reflectogram recorded in NIR range and by subtracting it from the measured values in the near infrared spectral sub-band. As an extrapolator we suggest a feed forward artificial neural network (ANN). Significant results of improved visualization are exemplified on reflectograms acquired with a VIS-NIR $\langle 400, 2250 \rangle$ nm scanning device on real paintings such as Madonna dei Fusi attributed to Leonardo da Vinci. Parameters of the method, artificial neural network and separability of used pigments are discussed.

1. Introduction

Infrared reflectography (IRR) is a technique established in the 1960s [1] for investigation of historical paintings. It consists of detecting the radiation scattered back from a painted surface in a spectral range starting at around 800 nm, immediately beyond the visible one. By means of such utterly non-invasive and non-contact examination technique, one can shed light onto the artist's original idea by visualization of either a preliminary sketch made by the painter on a preparation ground, prior to painting, or the so-called *pentimenti*, changes to the original project during painting construction made by the artist himself. The analyses of underdrawing and hidden layers (presence/absence and type) are essential for a historic/stylistic study and for attribution or fake identification of the artwork. The contrast between materials, which readily absorb light (or are transparent) within the IR range, and other materials that reflect it, allows the scientist to produce images that contain information on both details hidden to the naked eye and the chemical composition of the compounds constituting the analyzed artworks. Generally, increasing transparency of pigment layers as a function of increasing wavelength enables to visualize features of the surface and subsurface layers (retouches, mass losses, integrity of the paint layer, overpaintings) in order to monitor the level of degradation or previous interventions. IRR has continued to evolve thanks to the technological breakthrough/advance concerning detector improvements (e.g., from Vidicon tubes in the 60s to Silicon CCD cameras in the 80s and the InGaAs, PtSi, PbS arrays in 90s) and focusing optics. For this reason, not all IR systems that are based on different technologies have equal performances: their resolution (spatial, tonal or spectral) and spectral sensitivity (up to 1 or 2 micron for Silicon CCD and Vidicon, respectively) may vary greatly. Data interpretation is then conditional upon the instrument used to capture the reflectographic data.

In the late 1990s the method expanded into the non-invasive multispectral imaging. This approach consists in collecting the backscattered signal in many adjacent spectral windows and offers many advantages with respect to the traditional single spectrally wide system. Should the number of the spectral windows be greater than approximately hundred, the method can be defined as a hyperspectral imaging. In any case, the two-fold character of the obtained data, in spectral and spatial domain, allows for chemical and spatial characterization of the materials employed to create artworks such as the pigments or binders [2–18]. The scope of this work is:

* Corresponding author.
E-mail addresses: blazek@utia.cas.cz (J. Blažek), jana.striova@ino.it (J. Striová), raffaella.fontana@ino.it (R. Fontana), zitova@utia.cas.cz (B. Zitová).

http://dx.doi.org/10.1016/j.dsp.2016.09.007
1051-2004/

- To demonstrate a new method of digital image processing that improves the visibility of concealed features in NIR reflectograms and thus improves the comprehensibility of the collected multispectral data set.
- To suggest an algorithm following the proposed method.
- To quantitatively describe NIR and VIS separability limitations.

In published papers a similar task has already been addressed, for example by means of VIS-NIR multispectral analysis or Raman and XRF imaging, solving the identification of painted layers [19,20] and used pigments [21], performing pigment segmentation [22,23] and classification [24–26], layer separation [27] by difference visualization [28] or by image enhancement methods [29], or composition change detection [19]. In general digital image processing methods (DIP) can produce more comprehensible images providing the art investigator with better insight into a painting.

2. Samples and artworks

2.1. Samples

A set of 132 mock-ups, either on wooden or canvas support, was used for this research. In specific, series of mock-ups simulating paintings on wooden desk were prepared in 1994 in the Opificio delle Pietre Dure and therefore properly naturally aged. The pigments, purchased as powders from Zecchi (Italy), were applied with egg tempera (50% egg yolk, 25% egg white, 25% vinegar) and oil binding medium on wooden panels with a preparation layer composed of gypsum and animal glue (rabbit skin glue dissolved in water in 1 : 16 ratio). Furthermore, all the mock-ups included underdrawings [30].

Additional mock-up samples were chosen from the M3art database [31], prepared to imitate gothic to baroque Italian paintings. The 4×4 cm squares of different colors were painted on white canvas using animal glue as a binding medium for the gothic to renaissance period. The composition of the color layer was constant for all mock-ups: 2 g of pigment for 10 drops of 5% solution of animal glue, 5 drops of turpentine, 3 drops of egg yolk and 1 drop of ethanol. The white canvas was prepared by mixing 3 volume parts of Bologna chalk (calcium sulfate), 2 volume parts of 7% aqueous solution of gelatin, 1 egg yolk and $\frac{1}{4}$ volume parts of polymerized linseed oil. The right half of each square color sample contained underdrawings.

2.2. Artworks

A brief description of the three case studies, on which the developed algorithm was tested, is given.

The first one is a non-assigned gothic painting of Golgotha. It is a tempera painting on wood. Size of the processed area is about 6×6 cm. The processed image was captured by a standard digital single lens reflective (DLSR) camera Canon D500 with removed infrared filter covering the CCD. Color depth was 8 bits. Range of NIR spectral window was $\langle 720, 1050 \rangle$ nm.

The second one is a 'Still life' from the Fine Arts Museum of Asturias, in the north of Spain. It is an early 20th century anonymous oil on canvas painting (23.4×28.4 cm). It represents a series of pottery, in a very centered composition, made with three different ceramic techniques: the first with a green tone, the second very glossy and the third on the part in the left side, in satinated brown. The background is plain to highlight the figures acting as protagonists on the canvas. Analysis with IRR reflectography revealed the top layer to be painted with red ochre, green earth, and lead white pigments. The presence of underpainting and underdrawings was discerned as well.

The third example subjected to feed forward ANN testing is the 'Madonna dei Fusi' (Madonna of the Yarnwinder). It is an oil on panel painting, realized between the years 1501–1507, attributed to Leonardo da Vinci, possibly with the contribution of one of his pupils. The painting is privately owned. It was restored at least twice, however previous attempts cannot be excluded. IRR revealed different pentimenti in the preparatory drawing.

Reflectographic images on the 20th and 16th century paintings, as well as on mock-ups, were recorded by means of the VIS-NIR multispectral scanner with a single point measurement of reflectance with perfect registration of each pixel as a function of wavelength. The instrument was described in detail elsewhere [5,32]. In brief, the detecting system consists of Si (for $\langle 380, 1000 \rangle$ nm range) and InGaAs (for $\langle 1050, 2500 \rangle$ nm range) detectors equipped with interferential filters yielding 32 channels (16 channels in the VIS range $\langle 380, 780 \rangle$ nm and 16 channels in the NIR range $\langle 750, 2500 \rangle$ nm). The spectral resolution, determined by the filter FWHM, is 20–30 nm and 60–120 nm in the VIS and NIR range, respectively. As a result, 32 spatially registered images at different wavelengths $\langle 400, 2500 \rangle$ nm were collected completing a hypercube of spectral and spatial information.

3. Method

The fundamental idea justifying our method development is based on the fact that some information content of the NIR reflectogram cannot be estimated from the VIS reflectogram. We assume a match of such estimated NIR values and measured NIR values, indicating the absence of any additional *layer*. Contrarily, when the estimation does not match the measured values, the resultant error is assigned to an extra *layer* affecting the response in the NIR.

3.1. Definitions

Due to the terminology interference between art and IT experts we start with definitions of terms used in this paper.

Definition 1. As a *spectral window* centered in wavelength λ with defined width w we understood a radiometric sub-band where density of radiation wavelengths in range $\langle \lambda - w, \lambda + w \rangle$ is significantly higher than density of other wavelengths. Moreover, density function is increasing at $\langle -\infty, \lambda \rangle$ and decreasing at $\langle \lambda, +\infty \rangle$.

For our purpose it is not necessary to define "significantly higher" in practice this parameter is defined by screening equipment (filter transmittance, sensor sensitivity, light source radiation density function).

Definition 2. A *layer* is a continuous volume of paint material (color, varnish, support, etc.), homogeneous in the sense of its optical properties.

Such *layer* does not necessarily correspond to the material used. We track the optical homogeneity which can vary in one material due to particle size, chemical modification on its volume border, cracks or other inhomogeneities.

In the following text we distinguish between VIS and NIR reflectogram information content and their difference. Corresponding terminology – *visible cover* of a painting and the *information gain* – was defined as follows:

Definition 3. A *visible cover* for a given pixel is set of *layers* which contribute to the reflectance measured in visible spectrum.

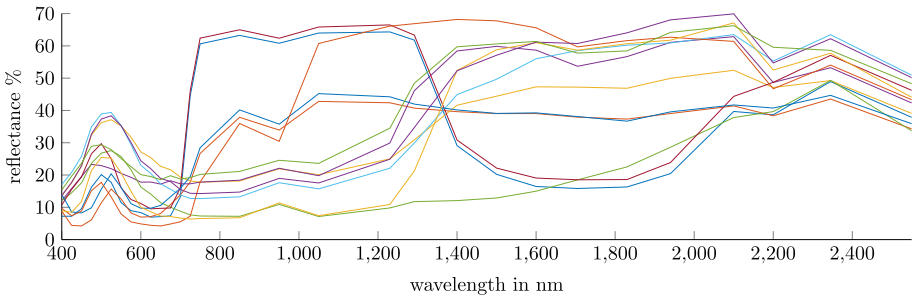

Fig. 1. Spectral responses of several green pigments in oil and egg tempera binding media. In the visible spectral range reflectance curves are very similar, whereas they vary much more in the near infrared range.

Thus the visible cover can contain for a given pixel more than one layer due to semi-transparency of the upper layer(s). This definition is not very intuitive but well describes reality where (in VIS) transparent, semi-transparent and opaque *layers* can be combined.

Definition 4. The *information gain* for a certain *spectral window* and a given pixel is the change in captured radiation caused by *layers* not included in the *visible cover*.

The *visible cover* affects the measured intensity the most because the level of absorption of upper *layers* weakens every effect of the *layers* below. In order to obtain *information gain* we need to suppress the *visible cover* effect in a *spectral window* reflectogram.

For similar tasks source separation methods are commonly used [29,33]. Often mentioned methods are *independent component analysis* from the group of blind source separation (BSS) [34–38], *principal component analysis* or other orthogonalizations. Application of source separation algorithms for the described problem is also possible here but has two limitations:

1. Optical model of a behavior of multilayer system is not linear [31]. Mixing model must take this into account. Most of BSS methods expects linear combination represented by mixing matrix, therefore results will not correspond with reality.
2. BSS methods expect that intensities measured in each subband are mixtures of *sources*. This presumption is too general. In our definition of the problem we refine this presumption into terms *visible cover* and *information gain* which we understood in BSS terminology as *sources*.

To conclude, a separation method should reflect the complexity of optical behavior of multilayer system that represent the typical painting structure [39]. For better comparison of our proposed method and BSS see section A.2.

The complexity of the addressed problem is demonstrated in Fig. 1, where the spectral reflectance factors measured in the range $\langle 400, 2250\rangle$ nm for several green colors is presented. The graph illustrates the typical behavior of paint materials: all measured spectral responses are very smooth. In spite of curves similarity in VIS range, in NIR range curves differ much more. Variances are:

$$\max_{\lambda\in\langle 400,700\rangle}(\sigma(I_\lambda)) = 0.1312, \tag{1}$$

$$\max_{\lambda\in\langle 700,2550\rangle}(\sigma(I_\lambda)) = 0.2203, \tag{2}$$

where λ is a *spectral window* central wavelength, I_λ denotes intensity measured in appropriate *spectral window* and $\sigma(I_\lambda)$ denotes standard deviation of intensities measured over all green colors (standard deviation per channel of constructed green phantom shows Fig. 6). VIS and NIR reflectance factors of one paint material correlate but do not relate on each other (both depend on paint material composition). Therefore an intensity relation $f : I(\lambda) \to I(\kappa)$ from *spectral window* λ to *spectral window* κ can be ambiguous if used paint material is impossible to be determined from the acquired dataset.

3.2. Proposed approach

A relevant estimation of the *visible cover* contribution in NIR reflectogram based on the visible spectral response is possible if and only if the set of materials is separable. Therefore existence of a transfer function $f : I(VIS) \to I(NIR)$, where I denotes the reflectance intensity is assumed.[1] To construct the best approximation f_T of this function f according to the collected pixels and their spectral responses, the pixels containing only the *visible cover* with no *information gain* were employed. Only this way extrapolated values containing minimum of *information gain* and maximum information pertinent to *visible cover* are obtained. Such set of pixels T belonging to K classes (according to *layer* content, i.e. optical properties) was used for the development of a f_T robust to noise:

$$T = \{C_1 \cup C_2 \cup \cdots \cup C_K\}, \tag{3}$$

$$C_i = \left\{p_{i,1}, \cdots, p_{i,|C_i|}\right\}, \tag{4}$$

$$I(p_{i,k}, NIR) = I(c_i, NIR) + n(c_i, NIR, k), \tag{5}$$

$$f : I\left(p_{i,k}, VIS\right) + n\left(c_i, VIS, k\right) \to I\left(p_{i,k}, NIR\right) + n\left(c_i, NIR, k\right), \tag{6}$$

where C_i is a set of pixels representing a material i. $p_{i,k}$ represents a pixel of the class C_i. c_i is a mean representation of the class C_i and $n(C_i, NIR, k)$ is a deviation of a pixel $p_{i,k}$ from this mean. Finally $I(p_{i,k}, NIR)$ is a reflectance intensity measured for a pixel $p_{i,k}$ in NIR range and n is a noise of C.

Being $f_T \sim f$, by using f_T spectral responses in the NIR *spectral windows* for all the pixels in the image can be extrapolated, creating a hypothetical image in the NIR *spectral window*, $\hat{I}_{NIR}$, containing only *visible cover*, which can be subtracted[2] from the measured data:

$$f_T(I_{VIS}) = \hat{I}_{NIR}, \tag{7}$$

$$\Delta = \left|I_{NIR} - \hat{I}_{NIR}\right|. \tag{8}$$

With suitable scaling of *information gain* Δ, an enhancement of hidden details is obtained.

3.3. f_T construction by feed forward ANN

For purpose of method demonstration, feed forward artificial neural network (ANN) for f_T construction was selected. An ANN

[1] This assumption is not valid but will be discussed in section 4.3.
[2] Subtraction is one possibility. We plan to focus on this problem in future.

Fig. 2. Example of virtual phantom. A simulation of image in spectral window with central wavelength $\lambda = 1750$ nm. Left: a phantom with additive noise; middle: phantom without noise – mean values for each paint material or paint material with underdrawing (right border); right: generated noise (variance used according to variance of real samples). Each horizontal line represents one paint material. On the right border is a simulated underdrawing. Noise image shows that the variance of each paint material differs and also that variance of combination of paint material with underdrawing is higher than that of poor paint material.

provides sufficient performance and ability to show the limitations of the method. Moreover:

1. No classification is needed. We do not want to work directly with C.
2. Produced f_T will be robust with respect to noise and to outliers, and has sufficient performance for separable sets of material.

There are several alternatives for f_T construction such as: Associative Memories Networks with various architectures [40,41], Support Vector Machines [42], Regression tools [43]. More can be found in [39].

Proposed feed forward ANN is based on the model of associative memory returning $c_i(NIR)$ for $c_i(VIS)$. The used associative memory divides space into polygons, where each polygon represents one pattern. This memory type is especially suitable for a high number of outliers included in data set and an a priori unknown number of classes K (number of used pigments and their mixtures).

A standard feed–forward ANN working with sum square error[3] was used. The proposed ANN has an input layer with 16 neurons accepting the reflectance in 16 sub-bands of the visible part of the spectrum and output layer has also 16 neurons corresponding to 16 sub-bands of near infrared spectrum. Various numbers of layers (from 1 up to 10) with various width (from 5 up to 1000 perceptrons) were examined in the testing phase. Each layer has sigmoid transfer function except for the last one where each neuron produces only linear combination of its inputs. For training the scaled conjugate gradient algorithm included in Matlab™ train function *trainscg* was employed, where 70% of samples were used for training, 15% for testing and 15% for validation of learning progress. Learning process was stopped when number of iterations exceeds 10000 or when 6 validations failed or the performance of ANN decreased[4] under 10^{-8}.

4. Calculations and method limitations

For testing the limits of proposed method several parameters were considered:

1. The size of scanned artwork
2. The number of used materials
3. VIS based separability of used materials
4. Pixel with non-zero *Information gain* coverage ratio

For each variable, several ANNs (20–25) were trained to result in the best performance; the training being performed on fully controlled virtual phantoms (Fig. 2). They were created in compliance with measured paint materials mean reflectance μ and variance σ^2 that were acquired from samples simulating a real painting (mentioned in section 2.1), used in the previous research [30,31].

$$\mu(\lambda, m) \sim avg\,(I(\lambda, m)) \tag{9}$$

$$\sigma(\lambda, m)^2 \sim var\,(I(\lambda, m))\,. \tag{10}$$

The virtual phantom was then created as follows:

1. A width S in pixels, a number of materials used $N < \|M\|$ and an underdrawings *coverage* $q \in \langle 0; 1\rangle$ were defined.
2. A height of the phantom was set as $\lfloor S/N \rfloor \cdot N$, where each $\lfloor S/N \rfloor$ line corresponds to one material
3. Finally, pixels were set as follows:
   (a) From the spectral database specified number of materials were randomly selected and both versions, without and with underdrawings ($m_C, m_D \in M$) were used.
   (b) Pixels in a row were set with the normal distribution corresponding to the material database records. Last $\lfloor S \cdot q \rfloor$ columns have distribution $\sim \mathcal{N}(\mu(\lambda, m_D), \sigma(\lambda, m_D)^2)$ and first $\lceil S \cdot (1-q) \rceil$ columns $\sim \mathcal{N}(\mu(\lambda, m_C), \sigma(\lambda, m_C)^2)$

The created phantom a has matrix size $(\lfloor S/N \rfloor * N, S, 32)$. Constructed virtual phantoms, reflecting the parameters of multispectral dataset of a real painting, had the following properties: $N = 12$, size $10k - 4M$, $q = 0.02$.

4.1. Effect of phantom size

Tests of the algorithm on real paintings revealed that size of the region on which ANN is trained influence the output quality demanded. The quality of extrapolation decreases as a function of the increasing size and hidden information disappears from an output image. Thus the first experiment is testing the hypothesis.

Hypothesis 1. The size of the processed area (used for the training and the estimation) affects the quality of an approximation.

[3] Improvements here are possible – sub-bands near to VIS spectral band should be estimated better than further sub-bands moreover another metric can be used or architecture can be changed to recurrent network.

[4] Performance stop case never happened.

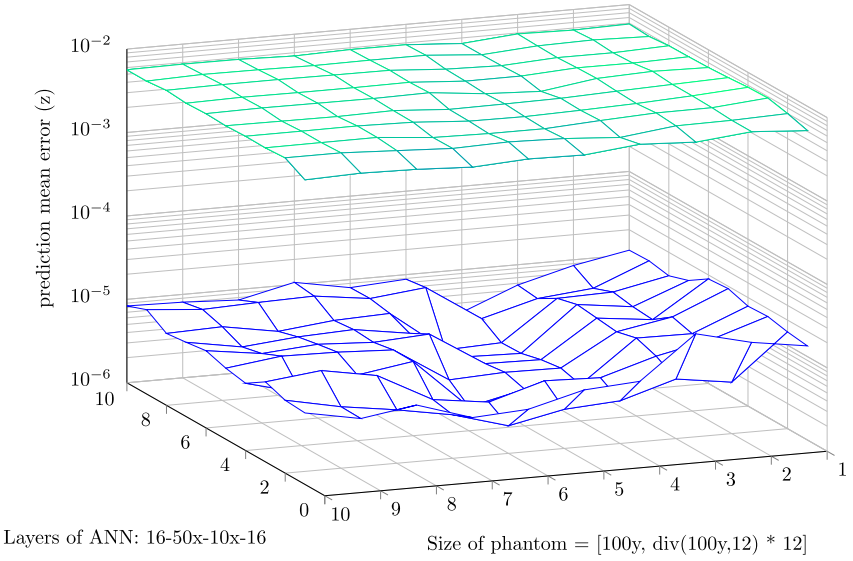

Fig. 3. Error in extrapolation as a function of the phantom size. Green upper mesh shows the error in the case of underdrawing present, blue bottom mesh is error between estimated and real reflectance values. Both graphs have similar shape (z-axis is logarithmic) with local minima for phantom size of 400×400 pixels due to the limitation of training samples to $50k$. The error behavior along the layer width axis shows that ANN performance does not increase as a function of growing network. (For interpretation of the references to color in this figure legend, the reader is referred to the web version of this article.)

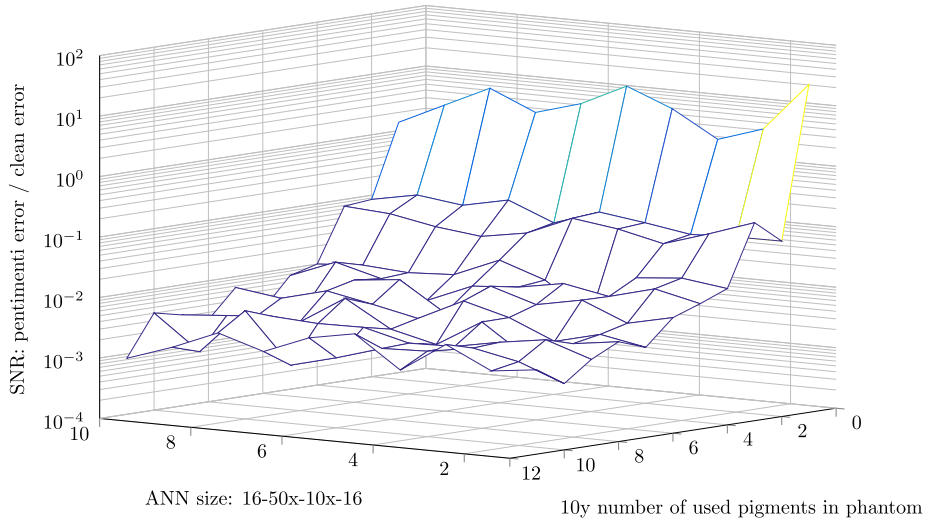

Fig. 4. Extrapolation error according to number of used pigments and ANN width. Mean error of the extrapolation "from VIS to NIR" per material and NIR sub-band. Error is computed according to the number of materials used (y axis) and ANN layer width (x axis). Graph shows that separability of materials used is limited – more materials cause cross-talks in the network and the overall performance decreases. More neurons in the layers cannot fix this problem.

We developed phantoms with size $S = k \cdot 100$, where $k \in 1, 2, \cdots, 20$, *coverage* $q = 0.02$ and number of used materials $N = 12$. Fig. 3 shows resulting graphs, which disapproves the Hypothesis 1. The performance of ANN does not decrease as a function of the growing processed area, however the minimal network size (> 250 neurons for 12 materials) should be kept.

4.2. Effect of used materials

The second experiment ($S = 500$, $q = 0.02$ and $N = 10k$, where $k \in 1, \cdots 11$)[5] was performed to clarify whether or not the ANN efficiency decrease is caused by greater variability of reflectance intensity values (due to increasing number of materials in analysis) in the processed area.

Hypothesis 2. The number of materials present in the processed area affects the performance of ANN.

Results of this experiment (Fig. 4) show that performance of ANN with two inner layers (four in total) is negatively affected by increasing number of materials. Performance improvement by using ANN architecture with more layers was tested as well (see Fig. 5) (with $S = 500$, $q = 0.02$, $N = 10k$ for $k \in 1, \cdots 12$ and the number of layers goes from 1 to 10, each layer has 20 neurons). Increasing the layers amount shows a partial improvement of ANN performance, however is not applicable in practice. The curve representing the performance dependence on ANN depth and the number of materials is hyperbolic like (see Fig. 5) thus the same performance for more materials requires extra hundreds of layers which are hardly trainable in real-time.

The presented graphs show that the paint material variability in the processed area is the most limiting factor for the method

[5] Materials was randomly selected for each training.

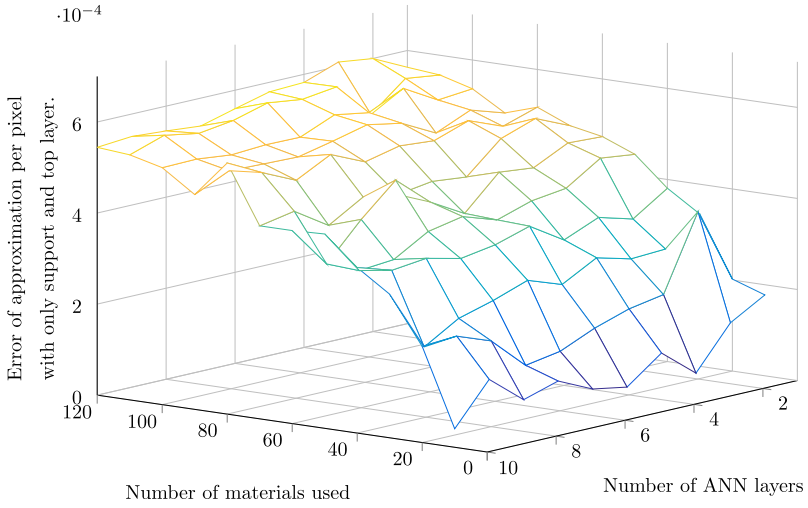

Fig. 5. Error in extrapolation according to pigments used and ANN depth. Error in extrapolation VIS to NIR, mean per material and NIR sub-band, according to the number of materials and the number of ANN layers. Graph shows that separability of materials used can be improved by more layers in ANN on the other hand the number of layers and neurons grows much faster than the number of separable materials.

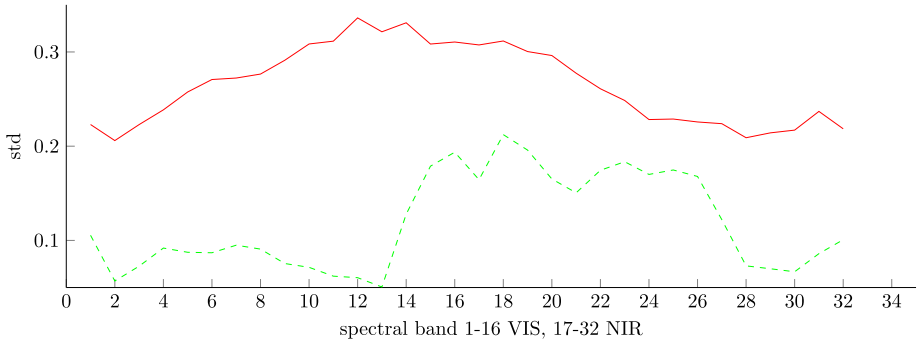

Fig. 6. Standard deviation of pixels on the whole phantom, all pigments together. Green dashed line correspond to inseparable green phantom and red solid line to rainbow phantom. Bands from 1 to 16 represent VIS part of spectra, 17–32 NIR part of spectra. Difference between phantoms is clearly visible. (For interpretation of the references to color in this figure legend, the reader is referred to the web version of this article.)

performance. If the difference of the estimated values and measured intensities is similar for pixels used for training as well as for analyzed pixels with pentimenti the increase of the painting comprehensibility is negligible. On the other hand, as long as the variability of area does not affect separability (Fig. 4, 5), useful results can be achieved with relatively small number of neurons in ANN. Training of such small ANN is fast and easily applicable in practice.

4.3. Separability

It was demonstrated that the increasing number of used materials negatively affects the performance of ANN in spite of the growing size of ANN. One possible explanation is the separability of materials in VIS. When two materials have the same spectral response in the VIS (same color), ANN is not able to distinguish between them and a prediction for NIR will be the same for both materials. During the learning phase, the estimation of ANN can either converge to some weighted mean value or completely diverge. In both cases (convergence or divergence) the final estimation will not be correct. Following hypothesis should be verified:

Hypothesis 3. When materials in VIS behave similarly, they will be inseparable for ANN. The growing size of ANN does not increase the performance.

For testing Hypothesis 3, two phantoms were prepared, both with fixed number of colors $N = 12$. Green colors from Fig. 1 and rainbow colors with varying VIS spectral response were used for the first and second phantom, respectively. Standard deviation of green and rainbow phantom intensity values is depicted in equations (1), (2). (The variations of intensity values per spectral subband for both phantoms are in Fig. 6.) The *coverage* was set to $q = 0.02$ and ANN layers width spans from $[16 \to 5 \to 1 \to 16]$ neurons to $[16 \to 100 \to 20 \to 16]$ neurons in individual ANN layers. An approximation for the rainbow phantom improves with an increase of ANN size, whereas for the green one the best approximation is reached with $[16 \to 25 \to 5 \to 16]$ neurons (see Fig. 7).

It is apparent that a key parameter, determining the size of the area to be processed by our algorithm, is the separability of materials in VIS. (However, this parameter is difficult to define or to estimate.)

For real paintings, the problem of the material separability is of minor issue. In fact, limited number of separable materials, of different visible spectral response, is usually used. The separability can decrease for the mixtures of materials that may have the spectral characteristics different from those of the pure colorants. A proposed workaround for such situation consists in processing areas not larger than 15×15 cm. It follows that small ANN, fast in the learning process, can provide satisfactory output. The optimal size of the processed area should depend then on the separability of used materials and on their mixtures.

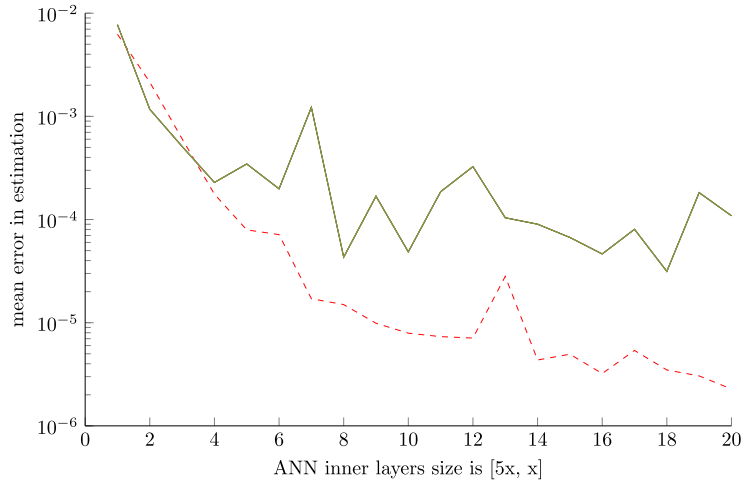

Fig. 7. ANN performance for 12 materials. Performance of ANN on rainbow phantom representing well separable set of materials (red dashed line) and green phantom representing inseparable set of green materials (green solid line) 1. (For interpretation of the references to color in this figure legend, the reader is referred to the web version of this article.)

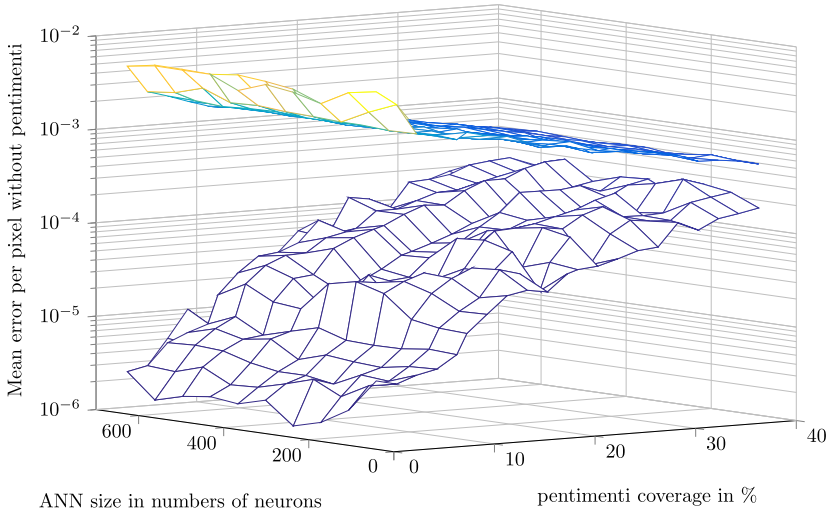

Fig. 8. Error in extrapolation when the coverage grows. Bottom mesh describes the mean error per coverage and ANN size for pixels without underdrawings – this should be minimized. Upper mesh describes mean error for pixels with pentimenti – this should be maximized. When the coverage grows, both errors are closer and as a result, pentimenti are less distinguishable.

4.4. Coverage effect

This work is focused on sparse areas like pentimenti, retouches, etc. which cover no more than 2% of a scanned area. Our last experiment describes what happen if all the pixels of the reflectogram (with non-trivial *information gain* included) are used for the training of ANN. By using of all the pixels necessary expert user interaction for sample selection is eliminated and the processing will be fully automatic.

A set of phantoms ($S = 500$, $N = 12$, and $q = 0.02k + 0.01$, where $k \in 0, \cdots, 19$) were created and all the pixels of the phantom were used for training of ANN. The ability of the extrapolator to distinguish between pixels with and without *information gain* is presented in Fig. 8. This ability corresponds to the distance between the node of the top and the bottom mesh in the figure. Indeed, the growing *coverage* q increases the necessity of purposefully selected training samples. In Fig. 8 pixels with non-zero *information gain* are represented by upper the surface and pixels containing only *visible cover* by the bottom surface. When coverage grows ANN recognition decreases, as both surfaces are closer. The growing size of the neural network does not compensate the ANN recognition ability.

5. The results obtained on artworks

This section presents three illustrative examples of real paintings on which our method was tested.

In the first experiment, a standard DLSR camera without infrared filter was used to capture RGB and $\langle 700, 1050 \rangle$ nm NIR images of a Gothic painting. The estimator was a feed forward ANN with $3 \to 50 \to 10 \to 1$ neurons. The processed image had 800×800 pixels and all the pixels were used for training. The results (Fig. 9) show that the most emphasized areas (black and white parts) are caused by spatial registration misalignment of RGB and NIR images. On the other hand, required demanded *information gain* enhancement was achieved: a contour on the top of the head (highlighted in the blue square) is not apparent either in VIS or in NIR image.

In the second experiment, a 32 band multispectral data set of a modern canvas painting measured by VIS-NIR scanner [5,32] was analyzed. The selected input had 16 bands in VIS $\langle 400, 700 \rangle$ nm with a 25 nm step. Estimating ANN has four layers with $16 \to 25 \to 25 \to 1$ neurons, the chosen processed area had 312×394 pixels size that were also used for training. The extrapolated and enhanced output band was a *NIR spectral window* centered at

Fig. 9. A Gothic painting as captured by DLSR camera. Left: RGB image, middle: NIR image, right: output of our algorithm. The images were processed all at once (original size $800 \times 800 px$). In the blue squares are details scaled for better visibility. (For interpretation of the references to color in this figure legend, the reader is referred to the web version of this article.)

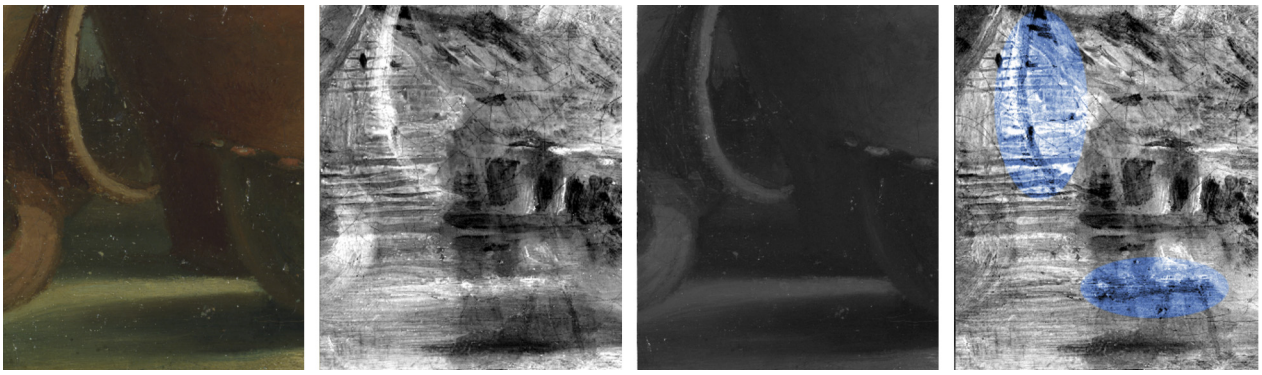

Fig. 10. Experiment with an early 20th century anonymous canvas painting. Left: RGB image, middle left: reflectogram measured at central wavelength $\lambda = 1200$ nm, middle right: output of ANN extrapolation, right: a difference between middle left and right images (*information gain*). Blue areas highlights uncovered areas with significant *information gain*. Note: Contrast of the second and the fourth images was expanded for better visibility and comparison. (For interpretation of the references to color in this figure legend, the reader is referred to the web version of this article.)

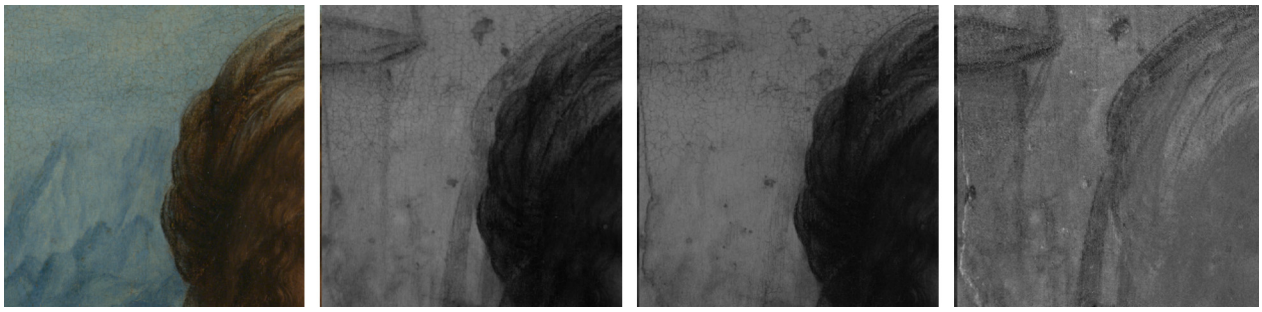

Fig. 11. Experiment with the 16th century wooden desk painting attributed to Leonardo da Vinci. Left: RGB image, middle left: a reflectogram centered at wavelength $\lambda = 1050$ nm, middle right: output of ANN extrapolation, right: difference between the measured and the extrapolated outputs; the *information gain*. (For interpretation of the references to color in this figure legend, the reader is referred to the web version of this article.)

1200 nm as shown in Fig. 10. Information uncovered by the algorithm is evidenced with blue color. The unveiled contours are invisible in the NIR reflectograms because concealed by an NIR low transparent *visible cover*.

In the third experiment, another multispectral dataset of a painting on wood with date inscripted on the 15th century was addressed. In agreement with the previous experiment, a selected input for ANN consisted of 16 VIS bands and all 16 IR $\langle 750, 2550 \rangle$ nm bands were extrapolated and *information gain* computed and enhanced.

Estimating ANN had four layers with $16 \rightarrow 25 \rightarrow 25 \rightarrow 16$ neurons. The processed area had a size of 300×300 pixels and all of them were involved in training. This experiment (Fig. 11) shows that the highest efficiency of extrapolation is achieved with the highest variability in reflectance intensity values in VIS. The structures masked by *visible cover* in right part of the image were successfully uncovered.

Recommendations for the data processing based on the experimental evidence can be summarized as follows:

- The *visible cover* of the painting should not be homogeneous. Higher variance of the *visible cover* increases the separability of the classes (see Fig. 11).
- Studied infrared reflectogram should contain at least some visible structures. The method cannot achieve results behind the

scope of reality, it can only accentuate present information and improves its comprehension.
- Analyzed images must be spatially registered. On the misalignment, black and white lines appear on edges in the painting (see Fig. 9).

6. Discussion

In general, the proposed algorithm is well suited for the enhancement of individual detail of painting (from 100*k* pixels up to 1 *Mpx*). However, it is not meant for processing full size images. Using smaller size of processed area leads to emphasizing the noise, due to the worse ANN generalization; larger patches approach is not time-effective. Therefore, the selected size of the area to be processed (as well as ANN number of layers and their width) defined by user should reflect the material separability. For similar colors in VIS smaller areas should be processed whereas for the well separable colors larger areas can be used (code for testing [44]).

Possible improvement can be achieved by other choice than subtraction for the construction of the *visible cover* estimation (equation (8)). The more complex model should be based on the optical behavior of individual *layers*, better reflecting properties of the used materials. This approach will be subject of our future research.

There exist possible generalization of the method for other spectral ranges combining *visible cover* and non-trivial *information gain* acquired in modalities like X-ray, ultra-violet fluorescence or terahertz imaging. The method workflow remains the same and quality of results will be related to the correlation of target modality and VIS modality. Higher correlation means worse visibility of hidden features on a modal image but with good ANN based estimation more distinct visualization will be achieved. ANN estimation performance depends mostly on coverage factor q in training set of pixels.

7. Conclusion

We have presented a new algorithm for information enhancement on multispectral data sets. Spectral imaging technology has recently gained importance in the analysis of ancient paintings. In particular, multispectral imaging in the near-infrared (NIR) and visible (VIS) region has proved useful for studying underlying features and for pigment identification, respectively. Because of the transparency of most pigments to IR radiation, NIR reflectograms can shed light onto the artist's original idea by the visualization of either the underdrawing or the so-called pentimenti. Depending on pigment transparency in the NIR spectral range, the acquired infrared images may partially contain information pertinent to the visible spectrum, decreasing, thus, their readability.

The new methodology consisted in suppressing VIS from NIR information content by extrapolating the reflectograms in the VIS to those recorded in NIR range and subtracting the extrapolated image from the measured IR one. As a result, separated information of the NIR is achieved.

The feed forward artificial neural network (ANN) algorithm for extrapolation was successfully tested on real paintings and a few examples were reported. The results of fully controlled experiments with virtual phantoms were also described to demonstrate the methodology limitations. In the ANN design, the effect of the number and width of the network layers was analyzed, as well as its effectiveness with respect to the number of neurons. The optimum was reached for two inner layers, which outperformed the three layers setting.

The implemented method in Matlab for processing of registered multimodal data sets is open access [44].

In the future we plan to focus on more profound analysis of the ANN setting and on a more accurate model of the optical behavior of multilayer systems.

Acknowledgments

We would like to thank to Janka Hradilová and Blanka Valchářová for the possibility capture photos presented in Fig. 9.

Access to computing and storage facilities owned by parties and projects contributing to the National Grid Infrastructure MetaCentrum, provided under the programme "Projects of Large Infrastructure for Research, Development, and Innovations" (LM2010005), is greatly appreciated. Without them this research cannot be possible.

The authors of INO would like to acknowledge the INSIDDE project (INtegration of cost-effective Solutions for Imaging, Detection, and Digitisation of hidden Elements in paintings), FP7-ICT-2011.8.2 ICT for access to cultural resources. Moreover, we thank Dr. Marta Florez Igual from the Museo de Bellas Artes de Asturias for providing us with the painting shown in Fig. 10.

The authors of IITA CAS would like to acknowledge the Czech Science Foundation, which has supported this work (project no. P103/12/2211).

Appendix A

A.1. Noise enhancement

One not yet mentioned problem of the proposed method is noise. The noise in the multispectral dataset can be independent for each spectral window (according to scanning technique). In such case the estimator f could not suppress it. When a feed forward ANN is used the noise is propagated through the network:

$$f_T\left(n(x_i)\right) = \hat{n}(y_i). \tag{11}$$

This give us in output image:

$$\Delta = \left(n(y_i) - \hat{n}(y_i)\right). \tag{12}$$

If the noise contains regular patterns (is dependent on a signal or correlates through different spectral windows), these patterns will be learned and suppressed. But in most cases the noise will be independent and e.g. randomly distributed according to a normal distribution:

$$n(y) \sim N(0, \sigma_{n_y}^2), \hat{n}(y) \sim N(0, \sigma_{n_x}^2). \tag{13}$$

In such case we obtain the noise level in the output image equal to

$$n(y_i) - \hat{n}(y) \sim N(0, \sigma_{n_y}^2 + \sigma_{n_x}^2). \tag{14}$$

It means that in the output image the noise will be enhanced too. The variance of the noise in the enhanced image will be the sum of variances of input data sets. The choice of suitable noise reduction algorithm is out of the scope of our article. The development of such algorithm should start with the noise distribution measurement. There are big problems in collection of measured samples and their connection with real paintings (aging effect, pigment mixtures, etc.). Moreover the normal distribution assumption can be violated.

A.2. Blind source separation

Common practice for information enhancement from IRR is usage of blind source separation (BSS) algorithms: PCA, ICA, orthogonalization [29,33], morphological component analysis (MCA) [38],

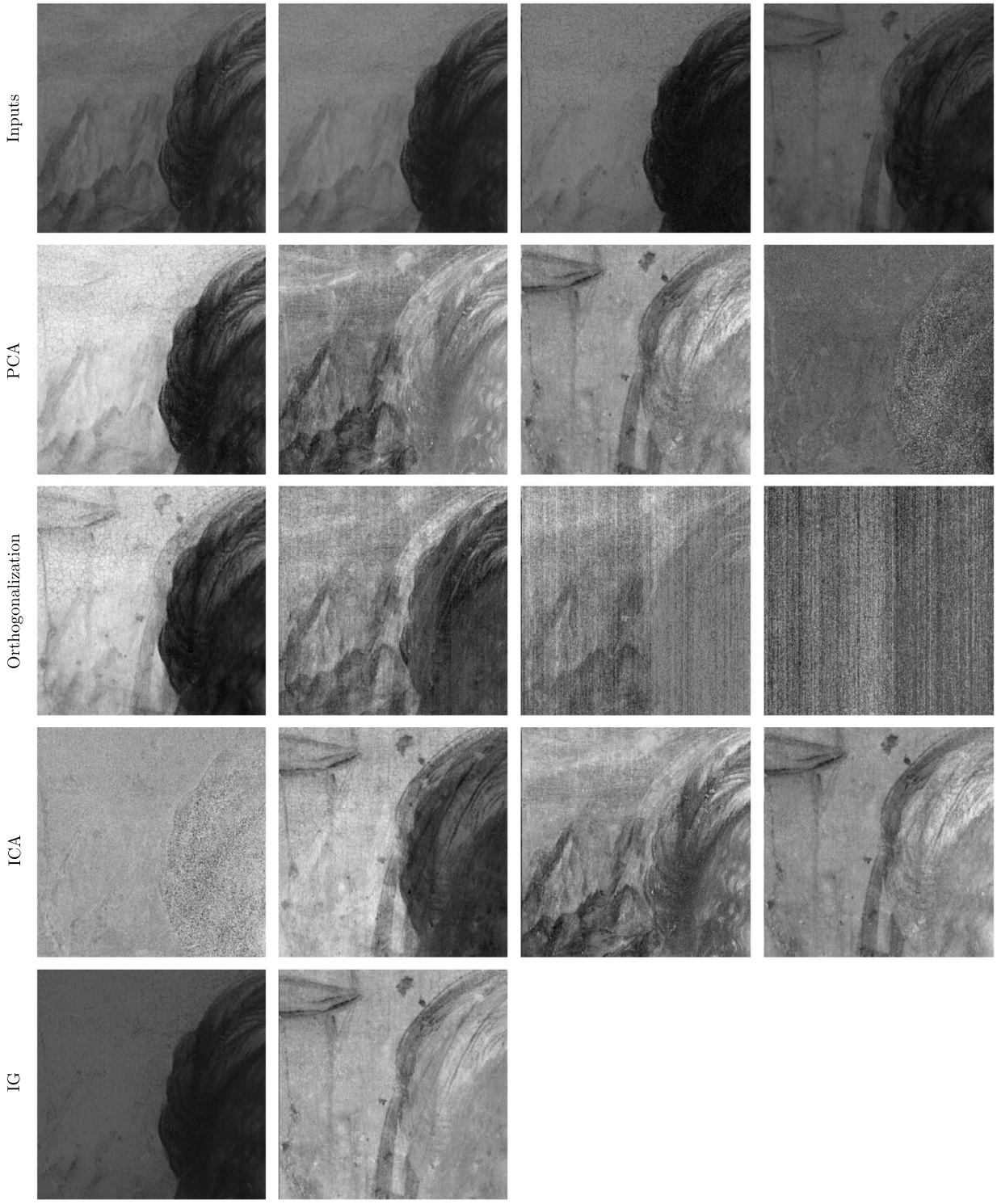

Fig. 12. Visual comparison of various source separation algorithms. First row presents reduced dataset to red, green and blue channel and spectral subband $\lambda = 1050$ nm. Second row shows PCA decomposition according to eigenvectors (Matlab function *pca* with *Algorithm* set to *eig*). Third row is orthogonalization by Matlab function *qr* and for the fourth row EFICA algorithm [45] was used. In the last row the same dataset was processed by our proposed method – left image shows extrapolation of RGB channels into NIR spectral subband, right image shows *information gain* i.e. difference between measured intensities of pixels and extrapolated values.

non-negative matrix factorization (NMF). Therefore we feel a necessity to put our method into this existing context. Following paragraphs describe how the proposed method and BSS relate and their pros and cons.

In the case of estimation of *information gain* in BSS terminology we have one known source signal $I(VIS)$ and one mixture $I(NIR) = \hat{I}(NIR) + \Delta$. Therefore there is no source separation just fitting of $\hat{I}(NIR)$, see equation (7). If we would like to use BSS algorithm for information enhancement we can state the problem as having two mixed signals $I(VIS)$ and $I(NIR)$ and set of unknown sources (typically number of sources is the same as input mixtures). Separation algorithm then creates, according to *contrast function* (for the definition see [37]), independent components.

Proposed algorithm has therefore these advantages:

- Interpretability. The resulting output image contains just the information gain of the specified modality and a noise. This minimizes possible misinterpretation. In the case of BSS methods the content range of a particular output image is set based on the statistical characteristic of the input data, not taking into account their physical interpretability.
- Enhancement. The information gain from selected modality is enhanced.
- Stability. Our proposed method converges to visually similar results through multiple runs and independently on the input content variation. The BSS methods generate a lot of noisy images (which are useless and can be dropped), often not ordered (for some methods orthogonal vectors can be produced in different order) and with badly set sign of the result (which is caused by the undefined orthogonal vector orientation). The stability of the BSS depends on selected *contrast function* [37].

There are the disadvantages of our proposed method:

- Noise enhancement. In BSS methods, noise and information are concentrated in different channels, whereas our proposed method do not remove noise into any specific channel, moreover its level can increase (see section A.1).

From these qualities we derive following guidelines for choosing the correct tool:

- BSS methods can be useful when:
  - The covered layer is partially visible in VIS. In such case measured $I(VIS)$ is also a mixture of unknown *sources*.
  - Input signals are relatively noisy. Noise can be separated as a source.
- The computation of *information gain* by our proposed method is useful when:
  - Studied layer content is invisible in VIS reflectogram. VIS can be classified as a source.
  - Misinterpretation is critical. BSS methods generates sources blindly and information from various modalities can be mixed, e.g. an edge split into VIS and NIR can be joined in one of BSS output source but not in *information gain* image.
  - Input signals have low level of noise.

Finally Fig. 12 contains an example of output of orthogonalization, PCA and ICA for comparison (as in [29] on reduced dataset from Fig. 11). We present, according to our decision, the best example where these methods generates comparable results as our proposed method.

References

[1] J.R.J. Van Asperen De Boer, Reflectography of paintings using an infrared vidicon television system, Stud. Conserv. 14 (3) (1969) 96–118.
[2] Kirk Martinez, John Cupitt, David Saunders, Ruven Pillay, Ten years of art imaging research, Proc. IEEE 90 (1) (2002) 28–41.
[3] Costas Balas, Vassilis Papadakis, Nicolas Papadakis, Antonis Papadakis, Eleftheria Vazgiouraki, George Themelis, A novel hyper-spectral imaging apparatus for the non-destructive analysis of objects of artistic and historic value, J. Cult. Heritage 4 (Jan 2003) 330–337.
[4] John K. Delaney, Elizabeth Walmsley, Barbara H. Berrie, Colin F. Fletcher, Multispectral imaging of paintings in the infrared to detect and map blue pigments, in: (Sackler NAS Colloquium) Scientific Examination of Art: Modern Techniques in Conservation and Analysis, Front Cover Proceedings of the National Academy of Sciences, Aug 16, 2005, National Academies Press, 2005, pp. 120–136.
[5] C. Bonifazzi, P. Carcagnì, R. Fontana, M. Greco, M. Mastroianni, M. Materazzi, E. Pampaloni, L. Pezzati, D. Bencini, A scanning device for VIS–NIR multispectral imaging of paintings, J. Opt. A, Pure Appl. Opt. 10 (6) (June 2008) 064011.
[6] Yonghui Zhao, Image segmentation and pigment mapping of cultural heritage based on spectral imaging, PhD thesis, Rochester Institute of Technology, 2008.
[7] Claudia Daffara, Enrico Pampaloni, Luca Pezzati, Marco Barucci, Raffaella Fontana, Scanning multispectral IR reflectography SMIRR: an advanced tool for art diagnostics, Acc. Chem. Res. 43 (6) (June 2010) 847–856.
[8] Claudia Daffara, Raffaella Fontana, Multispectral infrared reflectography to differentiate features in paintings, Microsc. Microanal. 17 (05) (Sep 2011) 691–695.
[9] Linda Cséfalvayová, Matija Strlič, Harri Karjalainen, Quantitative NIR chemical imaging in heritage science, Anal. Chem. 83 (13) (Jul 2011) 5101–5106.
[10] Haida Liang, Advances in multispectral and hyperspectral imaging for archaeology and art conservation, Appl. Phys. A, Mater. Sci. Process. 106 (2) (2012) 309–323.
[11] Paola Ricciardi, John K. Delaney, Michelle Facini, Jason G. Zeibel, Marcello Picollo, Suzanne Lomax, Murray Loew, Near infrared reflectance imaging spectroscopy to map paint binders in situ on illuminated manuscripts, Angew. Chem., Int. Ed. 51 (23) (June 2012) 5607–5610.
[12] Camille Simon Chane, Alamin Mansouri, Franck S. Marzani, Frank Boochs, Integration of 3D and multispectral data for cultural heritage applications: survey and perspectives, Image Vis. Comput. 31 (1) (2013) 91–102.
[13] M. Alfeld, J.C. Broekaert, Mobile depth profiling and sub-surface imaging techniques for historical paintings – a review, Spectrochim. Acta, Part B, At. Spectrosc. 88 (2013) 211–230.
[14] Francesca Rosi, Costanza Miliani, René Braun, Roland Harig, Diego Sali, Brunetto G. Brunetti, Antonio Sgamellotti, Noninvasive analysis of paintings by mid-infrared hyperspectral imaging, Angew. Chem., Int. Ed. 52 (20) (May 2013) 5258–5261.
[15] Alejandro Ribés, in: Advanced Color Image Processing and Analysis, Springer Science + Business Media, New York, NY, 2013, pp. 449–483, chapter 14.
[16] Kathryn A. Dooley, Damon M. Conover, Lisha Deming Glinsman, John K. Delaney, Complementary standoff chemical imaging to map and identify artist materials in an early Italian renaissance panel painting, Angew. Chem., Int. Ed. 53 (50) (December 2014) 13775–13779.
[17] Antonino Cosentino Panoramic, Macro and micro multispectral imaging: an affordable system for mapping pigments on artworks, J. Conserv. Mus. Stud. 13 (1) (Jul 2015) 1–17.
[18] John K. Delaney, Mathieu Thoury, Jason G. Zeibel, Paola Ricciardi, Kathryn M. Morales, Kathryn A. Dooley, Visible and infrared imaging spectroscopy of paintings and improved reflectography, Heritage Sci. 4 (1) (2016) 1.
[19] A. Gooch, J. Tumblin, Visualizing pentimenti: revealing the hidden history of paintings, J. Math. Arts 1 (June 2007) 133–142.
[20] Anila Anitha, Andrei Brasoveanu, Marco F. Duarte, Shannon M. Hughes, Ingrid Daubechies, Joris Dik, Koen Janssens, Matthias Alfeld, Virtual underpainting reconstruction from X-ray fluorescence imaging data, in: 19th European Signal Processing Conference, EUSIPCO, Barcelona, 2011, pp. 1239–1243.
[21] A. Del Mastio, A. Pelagotti, V. Cappellini, Multispectral and multi-modal imaging data processing for the identification of painting materials, in: Lasers in the Conservation of Artworks, CRC Press, August 2008, pp. 453–458.
[22] A. Pelagotti, A.D. Mastio, A.D. Rosa, A. Piva, Multispectral imaging of paintings, IEEE Signal Process. Mag. 25 (4) (2008) 27–36.
[23] Kathryn A. Dooley, Suzanne Lomax, Jason G. Zeibel, Costanza Miliani, Paola Ricciardi, Ann Hoenigswald, Murray Loew, John K. Delaney, Mapping of egg yolk and animal skin glue paint binders in early renaissance paintings using near infrared reflectance imaging spectroscopy, Analyst 138 (2013) 4838–4848.
[24] Alicia Jurado-López, María Dolores Luque de Castro, Use of near infrared spectroscopy in a study of binding media used in paintings, Anal. Bioanal. Chem. 380 (4) (2004) 706–711.
[25] V. Kokla, A. Psarrou, V. Konstantinou, Computational models for pigments analysis, Appl. Phys. A 90 (1) (2007) 15–22.
[26] R. Hedjam, M. Cheriet, Historical document image restoration using multispectral imaging system, Pattern Recognit. 46 (8) (2013) 2297–2312.
[27] J. Dik, K. Janssens, G. Van Der Snickt, L. van der Loeff, K. Rickers, M. Cotte, Visualization of a lost painting by Vincent van Gogh using synchrotron radiation based X-ray fluorescence elemental mapping, Anal. Chem. 80 (16) (2008) 6436–6442. PMID: 18662021.
[28] É. Baudrier, A. Riffaud, A method for image local-difference visualization, in: Ninth International Conference on Document Analysis and Recognition, vol. 2, ICDAR 2007, IEEE, 2007, pp. 949–953.
[29] S. Legnaioli, E. Grifoni, G. Lorenzetti, L. Marras, L. Pardini, V. Palleschi, E. Salerno, A. Tonazzini, Enhancement of hidden patterns in paintings using statistical analysis, J. Cult. Heritage 14 (3, Supplement) (2013) S66–S70, Science and Technology for the Safeguard of Cultural Heritage in the Mediterranean Basin.
[30] A. Aldrovandi, M.L. Altamura, M.T. Cianfanelli, P. Riitano, I materiali pittorici: tavolette campione per la caratterizzazione mediante analisi multispettrale, OPD, Restauro 8 (1996) 191–210, 101–103.
[31] J. Blažek, J. Soukup, B. Zitová, J. Flusser, J. Hradilová, D. Hradil, T. Tichý, M3art: a database of models of canvas paintings, in: Marinos Ioannides, Nadia Magnenat-Thalmann, Eleanor Fink, Roko Žarnić, Alex-Yianing Yen, Ewald Quak (Eds.), Digital Heritage. Progress in Cultural Heritage: Documentation, Preservation, and Protection, in: Lecture Notes in Computer Science, vol. 8740, Springer International Publishing, 2014, pp. 176–185.

[32] R. Fontana, M. Barucci, E. Pampaloni, J. Striova, L. Pezzati, From Leonardo to Raffaello: insights by Vis-IR reflectography, in: Interpretation of Fine Art's Analyses in Diverse Contexts, 2014, Acta Artis Academica, 2014, pp. 15–26.
[33] Gianfranco Bianco, Fabio Bruno, Anna Tonazzini, Emanuele Salerno, Pasquale Savino, Barbara Zitová, Filip Sroubek, Elena Console, A framework for virtual restoration of ancient documents by combination of multispectral and 3D imaging, in: Italian Chapter Conference 2010, Eurographics, pp. 1–7.
[34] A. Hyvärinen, J. Karhunen, E. Oja, Independent Component Analysis, vol. 46, John Wiley & Sons, 2004.
[35] P. Comon, Ch. Jutten, Handbook of Blind Source Separation: Independent Component Analysis and Applications, 1st edition, Academic Press, 2010.
[36] G. Chabriel, M. Kleinsteuber, E. Moreau, Hao Shen, P. Tichavsky, A. Yeredor, Joint matrices decompositions and blind source separation: a survey of methods, identification, and applications, IEEE Signal Process. Mag. 31 (3) (May 2014) 34–43.
[37] J-F. Cardoso, Blind signal separation: statistical principles, Proc. IEEE 86 (10) (1998) 2009–2025.
[38] J. Bobin, Y. Moudden, J.L. Starck, M. Elad, Morphological diversity and source separation, IEEE Signal Process. Lett. 13 (7) (July 2006) 409–412.
[39] Luis B. Almeida, Nonlinear source separation, Synthesis Lectures on Signal Processing 1 (1) (Jan 2006) 1–114.
[40] T. Kohonen, Self-organization and Associative Memory, 3rd edition, Springer-Verlag, Inc., New York, NY, USA, 1989.
[41] G.A. Carpenter, Neural network models for pattern recognition and associative memory, Neural Netw. 2 (4) (January 1989) 243–257.
[42] Y.W. Chang, Ch.J. Hsieh, K.W. Chang, M. Ringgaard, Ch.J. Lin, Training and testing low-degree polynomial data mappings via linear SVM, J. Mach. Learn. Res. 11 (August 2010) 1471–1490.
[43] G.A.F. Seber, A.J. Lee, Polynomial Regression, John Wiley & Sons, Inc., 2003, pp. 165–185.
[44] J. Blažek, Algorithm for invisible information separation in multimodal datasets, http://github.com/gimlidc/matlab/dip-toolbox.git, October 2015, An algorithm for multimodal artwork investigation, enhances the visibility of information hidden in various modalities.
[45] Zbynek Koldovsky, Petr Tichavsky, Erkki Oja, Efficient variant of algorithm fastICA for independent component analysis attaining the CramÉ r-Rao lower bound, IEEE Trans. Neural Netw. 17 (5) (2006) 1265–1277.

Jan Blazek is a Ph.D. student at Charles University, Prague, Czech Republic. He obtained the M.Sc. degree, in 2009, at the same university at the faculty of Mathematics and Physics. Since 2010, he develops algorithms for digital image processing at Institute of Information Theory and Automation, Czech Academy of Sciences. During his Ph.D. studies he focus on application of visualization techniques, artificial intelligence and statistics in field of art investigation to support art conservators and restorers.

Jana Striova was born in Jicin, 1977, Czech Republic. She graduated, in 2002, at the Institute of Chemical Technology in Prague in Chemical Technology for the Conservation of Historical Monuments (M.Sc.) and, in 2004, at Kansas State University, USA, in Analytical Chemistry (M.Sc.). She obtained her Ph.D. (2009) in Science for the Conservation of Cultural Heritage (CH) at University of Florence, Italy, as a Marie-Curie Fellow. She has been a researcher at the National Institute of Optics CNR-INO in Florence, since 2012, after 2 years of postdoctoral fellowship at the Institute for the Conservation and Valorization of CH. Her research interest spans from the development and application of new spectroscopic and imaging techniques for examinations of artworks to the studies of novel cleaning systems applied in the field of cultural heritage. More generally, she focuses on setting-up of multianalytical protocols to probe non-invasively materials constituting artworks.

Raffaella Fontana was born in Pavia, Italy, in 1964. She graduated in Physics at the University of Florence, in 1992; she obtained the Ph.D. in Non Destructive Techniques, in 1997, at the Department of Electronic Engineering in Florence and the Post-graduation in Medical and Environmental Physics at the University of Florence, in 2000.

Since 2004, she has been working at INO-CNR (National Institute of Optics of the National Research Council) where she is Researcher. Since 2010, she is the Responsible for the Cultural Heritage Group of INO.

She is involved in many research projects in the field of optical technologies applied to Cultural Heritage. She is the scientific responsible for INO of the EU-project IPERION CH (Integrated Platform for the European Research Infrastructure ON Cultural Heritage, H2020-INFRAIA-1-2014/2015) and the EU-project INSIDDE (Integration of technological Solutions for Imaging, Detection, and Digitization of hidden Elements in artworks, FP7-ICT-2001-9). Her research activity concerns the study of methodologies, the development of optical techniques and instruments for the diagnostics of artworks, and the processing of both 2D and 3D data.

Barbara Zitova received the M.Sc. degree in computer science and the Ph.D. degree in software systems from Charles University, Prague, Czech Republic, in 1995 and 2000, respectively. Since 1995, she has been with the Institute of Information Theory and Automation, Czech Academy of Sciences. Since 2008, she has been the Head of the Department of Image Processing. She gives undergraduate and graduate courses on digital image processing and wavelets in image processing with the Czech Technical University and Charles University. Her research interests include geometric invariants, image enhancement, image registration and image fusion, and image processing applications in cultural heritage and medical imaging. She has authored/coauthored over 60 research publications in these areas, including monographs Moments and Moment Invariants in Pattern Recognition (Wiley, 2009) and 2D and 3D Image Analysis by Moments (Wiley, 2016).